Composites: Part A 76 (2015) 181–193

Contents lists available at ScienceDirect

Composites: Part A

journal homepage: www.elsevier.com/locate/compositesa

Solid-state additive manufacturing for metallized optical fiber integration

T. Monaghan *, A.J. Capel, S.D. Christie, R.A. Harris, R.J. Friel

Wolfson School of Mechanical and Manufacturing Engineering, Loughborough University, Loughborough, Leicestershire LE11 3TU, United Kingdom

ARTICLE INFO

Article history:
Received 13 January 2015
Received in revised form 27 April 2015
Accepted 3 May 2015
Available online 6 June 2015

Keywords:
A. Metal-matrix composites (MMCs)
A. Layered structures
A. Fibers
Ultrasonic Additive Manufacturing (UAM)

ABSTRACT

The formation of smart, Metal Matrix Composite (MMC) structures through the use of solid-state Ultrasonic Additive Manufacturing (UAM) is currently hindered by the fragility of uncoated optical fibers under the required processing conditions. In this work, optical fibers equipped with metallic coatings were fully integrated into solid Aluminum matrices using processing parameter levels not previously possible. The mechanical performance of the resulting manufactured composite structure, as well as the functionality of the integrated fibers, was tested. Optical microscopy, Scanning Electron Microscopy (SEM) and Focused Ion Beam (FIB) analysis were used to characterize the interlaminar and fiber/matrix interfaces whilst mechanical peel testing was used to quantify bond strength. Via the integration of metallized optical fibers it was possible to increase the bond density by 20–22%, increase the composite mechanical strength by 12–29% and create a solid state bond between the metal matrix and fiber coating; whilst maintaining full fiber functionality.

1. Introduction

Ultrasonic Additive Manufacturing (UAM) is a solid state metal Additive Manufacturing (AM) process that utilizes ultrasonic oscillations to bond metal tapes layer by layer before using periodic Computer Numerical Controlled (CNC) machining to fabricate complex three-dimensional components [1].

In UAM a rolling cylindrical horn, also known as a sonotrode, applies the ultrasonic oscillations generated by an ultrasonic transducer to the thin metal tapes (ca. thickness 50–200 μm). Due to sonotrode dynamics, ultrasonic oscillations and compressive normal forces applied through the sonotrode, interfacial stresses and intimate contact between mating foil surfaces are induced. This leads to disruption of typically stubborn oxide layers and induces both static and shear forces within the metallic foils. The result of which is elastic–plastic deformation of surface asperities, newly formed nascent surfaces and true metallurgical bonding between the foil and substrate [2–4]. A schematic of typical UAM processing equipment is detailed in Fig. 1. The strength and quality of the final part produced is directly related to several processing parameters controlled by the operator, including; normal force applied by the sonotrode (ca. 500–2000 N), traverse speed of sonotrode (ca. 10–100 mm/s), amplitude of sonotrode oscillation (ca. 10–50 μm), build platform temperature (ca. 25–200 °C) and the surface topography of the sonotrode [5,6].

The use of UAM in the formation of Metal Matrix Composites (MMC's) has been the subject of multiple studies [7,8]. The unique nature of the bonding mechanism within UAM makes it ideally suited to the manufacture of MMC's featuring both smart and passive integrated components. Firstly, the low temperatures associated with UAM allows for the incorporation of thermally sensitive components within solid metal structures. Metallurgical bonding at the weld interface can typically be achieved at temperatures approximately 30–50% of the matrix absolute melting temperature [5]. This reduction in processing temperature avoids thermal stresses arising from mismatches in the coefficients of thermal expansions as well as melt points – a common feature in other metal additive manufacturing processes [9,10]. Furthermore, as the deposited material is not elevated above its melt temperature, as is the case in powder bed fusion techniques such as Selective Laser Melting (SLM) and Selective Laser Sintering (SLS), issues such as embrittlement, residual stress and distortion of parts are significantly reduced. A second unique feature of UAM that makes it highly suitable for manufacturing MMCs is the large degree of localized plastic flow observed in the interlaminar region during foil deposition. This plastic flow allows for sound mechanical encapsulation of components by the matrix material [11]. To date, this ability has been utilized to incorporate a variety of fibers such as Silicon Carbide (SiC) for localized stiffening, Shape Memory Alloy (SMA)

* Corresponding author. Tel.: +44 01509 227586.
E-mail address: T.monaghan@lboro.ac.uk (T. Monaghan).

http://dx.doi.org/10.1016/j.compositesa.2015.05.032
1359-835X/

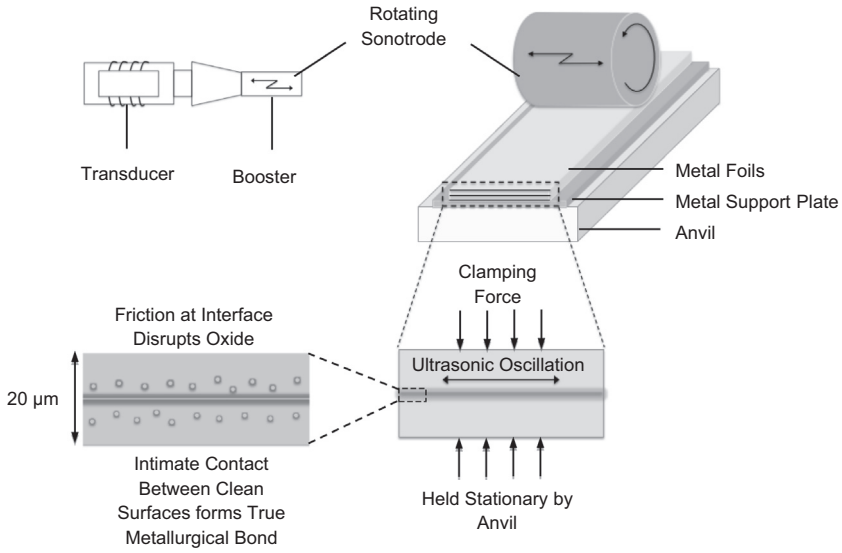

Fig. 1. Schematic diagram of a typical UAM set-up detailing the interfacial welding zone.

for actuation and optical fibers for sensing [12–14]. Other pre-fabricated components such as pre-packaged electronic systems and direct-written circuitries have been successfully incorporated into UAM structures [15,16]. For these reasons, UAM remains an appealing alternative to other higher temperature manufacturing techniques for manufacturing smart MMC structures.

The ability to successfully incorporate optical fibers within a metal matrix has the potential for application in areas such as structural fatigue/damage monitoring as well as real-time temperature, pressure and strain monitoring, in otherwise inaccessible locations [17,18]. Employing directly integrated fiber-optic sensors allows not only for potential reductions in component size and weight, they also benefit from increased corrosion resistant, greater immunity to electromagnetic interference and improved sensitivity. It is these qualities that often permit the use of fiber-optic strain sensors in a large variety of applications and harsh environments less suited to conventional resistive foil strain gauges. Their small size and geometric compatibility with composite materials allows them to be relatively non-perturbative when embedded, allowing for in situ strain monitoring within composite laminate structures and has led to their increased use in smart structure applications [17]. Previous work by Mou and co-workers demonstrated through thermal and loading responses of MMC's with embedded optical fibers containing laser etched FBGs embedded that they demonstrated self-sensing capabilities [18]. It was noted however that dissimilarities in the thermal expansion coefficient of the embedded FBG and surrounding matrix can lead to issues with FBG peak shifting as a result of similar expansion rates of the materials when subjected to heat. It was hypothesized that a different thermal sensitivity enhancement could be obtained if Aluminum were replaced with a different metal alloy with a substantially different thermal expansion coefficient. Yet, the work from Kong et al. still represents the most significant of its kind. A substantial contributor to the lack of following publications in this area is due to the frail nature of the UAM/optical fiber composite structures, post processing. In order for Kong to successfully encapsulate the silica optical fibers within the metal matrix, it was necessary to first remove the protective acrylic polymer coating surrounding the fiber [14]. Therefore, after successful encapsulation, the fibers often fracture at the weld interface when handled. Increasing the robustness of the fiber through the application of metallic coatings could potentially allow for the utilization of optimal UAM processing conditions. This in turn could lead to superior mechanical properties of the MMC structures produced.

Li and co-workers recently reported the application of Nickel coatings to optical fibers as a means of improving the durability of Fiber Bragg Gratings (FBG's) encapsulated through Ultrasonic Spot Welding (USW) [19]. Ultrasonic Spot Welding (USW) is a welding technique capable of joining non-ferrous similar and dissimilar metal components, at small localized points, through the use of high frequency sound energy to soften or melt the material under an applied pressure. Their results showed that through chemical-electroplating, a degree of protection can be afforded to the fibers from the spot-welding process with little or no effect of the wavelengths transmitted or the sensing capabilities of the fiber. These results are a good indication of the potential benefits of applying protective metal coatings to fibers prior to ultrasonic encapsulation, however spot welding itself is only capable of achieving small regions of consolidation in a static fashion – not large area bonding and continuous fiber integration that would be required for MMC manufacture.

As a result of this past work it would be pertinent to investigate both the effects of this protective fiber coating technique under UAM processing conditions and gain insight into how the ultrasonic fiber/matrix integration process performs in a continuous embedding manner as opposed to a singular spot-weld. This combination of UAM and metal coated optical fibers potentially allows the creation of more robust optical fiber based smart MMCs. The ability to embed optical fibers at a wide range of parameters, whilst still maintaining their functionality, has the potential to increase the scope of applications for UAM in the formation of the smart MMC structures. This paper is an investigation into the effect of UAM processing on metallized optical fibers (both Aluminum and Copper coated), the strength of the composite structures they yield, and how the UAM process performs in a continuous embedding manner on these fibers.

2. Methodology

2.1. Materials

Aluminum (Al) 3003 H18 foils, at ~100 μm thick and ~24 mm wide, were chosen as the matrix material in which the selected fibers were to be embedded. This material is readily available in

a foil format and its behavior under UAM processing conditions is well understood [1,5,20–22]. Two foils were ultrasonically welded individually onto an Al 1050 H14 support plate (~1.2 mm thick and ~30 mm wide) to form a UAM metal matrix. The physical properties of these two alloys are located in Table 1 along with their chemical composition [23].

Four metal-coated, graded-index, multimode optical fibers were chosen for this experimental series; Al 50–125, Cu 50–125, Cu 100–110 (IVG Fiber Ltd.), and Al 100–110 (AMS Technologies AG). These fibers consisted of two Aluminum-coated optical fibers and two Copper-coated optical fibers with analogous core sizes. Initially developed for ultra-high reliability telecommunications applications, these metallized fibers are also used for ultrahigh temperature monitoring, material fatigue monitoring and down-hole exploration in the oil and gas industry [24,25]. The central silica core sizes of these coated fibers represent the most common commercially available core diameters of uncoated optical fibers. Furthermore, they are of appropriate dimensions to be consolidated within UAM work piece, i.e. less than the thickness of the overlaying foil, and non-metallic coated equivalent fibers and cheap and readily available. The dimensions and compositions of these fibers are located below in Table 2.

In order to act as a reference, polymer coated optical fibers (Thorlabs Ltd.) with corresponding core sizes to the metalized versions were embedded (Table 3). This allowed for an evaluation of any potential change of matrix mechanical strength due to the application of a metallic support coating to the circumference of the fiber as well as giving a direct comparison by work conducted by Kong et al. who similarly used multimode optical fibers with 100 μm core diameters. The external coating applied to these silica fibers consists of an acrylate-based polymer intended to increase the durability of the rigid internal silica core. Despite the suitability of this coating to its intended purpose, the soft nature of this polymeric material results in its dispersion across the interfacial area between welded foils [14]. In order to combat this, the polymer-coated fibers were immersed in pure acetone for a period of 2 h to allow for removal of the protective layer.

2.2. Sample preparation

2.2.1. UAM equipment

All of the samples detailed in this paper were prepared using an Alpha 2 (Solidica Inc. USA) UAM machine located within Loughborough Universities Mechanical and Manufacturing Engineering department. This machine operates at a constant frequency of ~20 kHz, and utilizes a sonotrode with surface roughness (R_a) of 5.9 μm and a diameter of 50 mm.

2.2.2. Process chain of test sample fabrication

The process chain of sample fabrication is demonstrated in Fig. 2. The fiber embedded samples were prepared by first depositing two separate Al 3003 H18 foil layers onto an Al 1050 supporting plate, at 21 °C, to form a UAM metal matrix (Fig. 2a). Due to the total circumference of the coated fiber exceeding the thickness of a single Al 3003 foil, it was deemed necessary to deposit two foils. This ensured the fiber was interacting solely with Al 3003 and not penetrating the underlying foil and interacting with the Al 1050 base material. The welding parameters used for the preparation of these substrates were developed in house, and comprised of 1400 N weld force, 20 μm sonotrode amplitude and a weld speed of 40 mm/s.

Whilst previous work has been published regarding the optimum processing parameters of Al 3003 [5,26], it is often the case that UAM processing parameters require investigation for varying situations. Sonotrode geometry, material/substrate thickness and surface topography can all substantially alter the magnitude of friction and interfacial stresses at the sonotrode/foil and substrate/foil interfaces [27]. For this reason, the substrate preparation UAM parameters detailed above were selected based on the optimum welding parameters for the material composition and geometry with the UAM equipment possessed by the research group. The application of the third Al 3003 H18 layer varied as a result of the sample type being prepared. The parameters used to ultrasonically weld the third foil to the substrate were divided into two control parameter sets, one relatively high UAM processing parameter set and one relatively low UAM processing parameter set (Table 4).

The lower parameter (LP) set represents the upper limit of the process window developed by Kong et. al. in their work regarding the embedment of uncoated optical fibers via UAM into an

Table 3
Dimensions of acrylic coated optical fibers.

	50 μm Core fiber	105 μm Core fiber
Core diameter	50 μm ± 2%	105 μm ± 2%
Cladding diameter	125 ± 1 μm	125 ± 1 μm
Coating diameter	250 μm ± 5%	250 μm ± 5%

Table 1
Mechanical properties and chemical composition of Al 1050 H14 and Al 3003 H18.

	Al 1050 H14	Al 3003 H18
Density	2.71	2.73
UTS	100–135	200
Tensile yield strength	75	186
Modulus of elasticity (GPa)	69	68.9
Melting temperature (°C)	645–657	643–654
Composition (wt%)	Al (⩾99.08), Mn (⩽0.05), Cu (⩽0.05), Fe (⩽0.4), Si (⩽0.25), Zn (⩽0.07), Mg (⩽0.05), Ti (⩽0.05), Other (⩽0.03)	Al (96.7–99), Mn (1–1.5), Cu (0.05–0.2), Fe (⩽0.7), Si (⩽0.6), Zn (⩽0.1) Other (⩽0.15)

Table 2
Dimensions and coating compositions of metallized optical fibers.

	Al 50–125	Al 100–110	Cu 50–125	Cu 100–110
Primary coating	Aluminum (99.99% purity)	Aluminum (99.99% purity)	Copper (99.99% purity)	Copper (99.99% purity)
Core diameter	50 μm	100 μm	50 μm	50 μm
Cladding diameter	125 ± 1 μm	110 ± μm	125 ± 1 μm	125 ± 1 μm
Coating diameter	165 ± 10 μm	150 ± μm	165 ± 10 μm	165 ± 10 μm

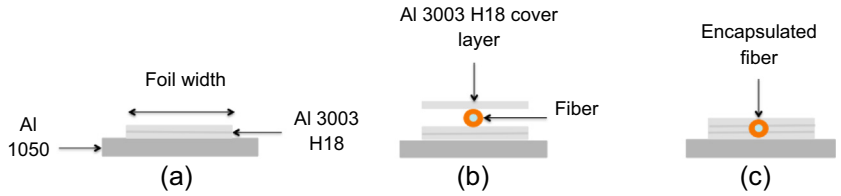

Fig. 2. Process chain of fabrication (a) Al 1050 a support plate with two bonded Al 3003 H18 foils (b) sandwich structure of un-embedded fiber between Al 3003 H18 foils (c) fully consolidated UAM matrix with completely encapsulated fibers. (For interpretation of the references to color in this figure legend, the reader is referred to the web version of this article.)

Table 4
Process parameters utilized in UAM sample fabrication.

	Low parameter (LP)	High parameter (HP)
Weld speed, mm s^{-1}	20	40
Weld force, N	1200	1400
Amplitude of oscillation, μm	12	20

Aluminum 3003 H18 matrix [14]. Attempting encapsulation above these parameters was shown to result in failure of the embedded fiber to transmit light due to fracturing of the silica structure. The higher parameter (HP) values, as noted previously, represent the optimum process parameters for the substrate and support material and were developed by the research group.

Both coated and uncoated optical fiber samples were prepared by placing a single 150 mm length of the specific fibers (Tables 2 and 3) along the direction of consolidation and fastened in place using temporary fixturing. The application of a third Al 3003 H18 foil layer then followed (Fig. 2b). The resulting sandwich structure was then consolidated with either LP or HP UAM parameters. (Fig. 2c). Monolithic samples (containing no fiber of any form) were prepared in order to act as a reference sample and highlight any potential effects on mechanical strength due to the inclusion of the fiber.

2.3. Fiber transmission testing

As stated previously, Kong et al. determined that above a certain UAM process parameter threshold (1200 N, 12 μm and 20 mm/s), embedded optical fibers were prone to light transmission failure (Section 1). To determine if the newly embedded metal-coated fibers were still capable of light transmission at the chosen UAM energy parameters, all fibers ability to transmit light post-encapsulation were investigated. This proceeded by coupling 25 cm lengths of the waveguides to a laser source (Orientek T15 M) and matching optical power meter (Orientek T25 M) via the use of a bare fiber adapter, in order to determine the power loss as a result of encapsulation. A total of three samples for each fiber and UAM energy combination were tested in this manner at two wavelengths (1301 nm and 1550 nm – determined by available equipment).

2.4. Topography of Aluminum substrate and embedded fibers

The topographies created in the UAM process for both monolithic and fiber embedded samples were analyzed using an Alicona InfiniteFocus IFMG4F surface profiling system and the acquired data was studied through the use of Talymap Platinum 5.0 software. In the UAM process, as the sonotrode passes over the underlying foil, surface deformation occurs creating a substrate surface similar in topography to that of the sonotrode itself due to a contact imprint being imparted from the sonotrode to the foil (Fig. 3).

The topography that results from direct sonotrode-foil contact has been shown to have a marked effect on the interlaminar

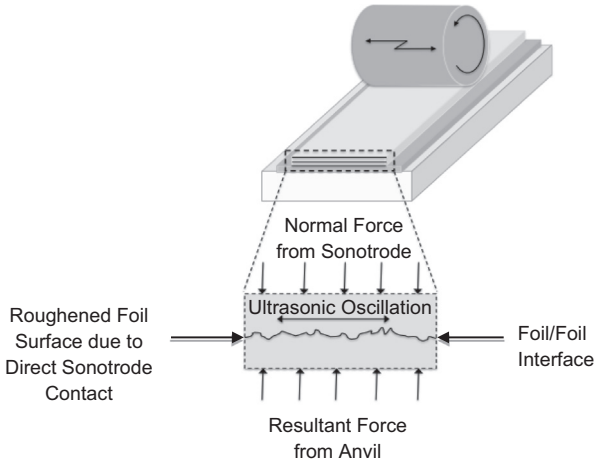

Fig. 3. Effect of sonotrode topography on the surface of newly consolidated foils.

bonding dynamics of a UAM structure [28]. By measuring the change in surface roughness as a result of embedding both coated and uncoated fibers, it is possible to predict the bonding characteristics likely to result from depositing a fourth layer on top of the covering layer (see Section 3.4). For both LP and HP UAM processing parameters, two samples were prepared for each fiber type, giving a total of 12 samples. The average surface roughness, termed R_a, was determined by analyzing a 10 mm long section of the surface making sure it encompassed the area directly over the embedded fiber. Three measurements were made for each substrate at the beginning, middle and end in order to gain an average for the surface as a whole. The settings of parameters used during topography measurement are stated in Table 5.

2.5. Assessment of bond quality and coating behavior

Assessment of the fiber–matrix bond interface was achieved through both microscopic cross-sectional examination and mechanical testing. Mechanical testing involved applying a load to the final Al 3003 cover foil in order to peel it from the underlying substrate (peel testing). Microstructure examination comprised of observing the plastic deformation of the matrix material around the embedded fiber. It is through this observation that an indication of the fiber–matrix interfacial bond quality can be assessed.

Table 5
Alicona InfiniteFocus parameter settings.

Measurement parameter	Setting
Exposure time	116 μs
Contrast	1.4
Vertical resolution	195 nm
Lateral resolution	3.91 μm
Magnification	10×

2.5.1. Peel testing

All peel testing performed in this work was done so in accordance with BS EN 2243-2 2005. By measuring a samples average resistance to peeling at the points of consolidation, it is possible to determine the consolidation strength between two foils. For each combination of UAM process parameters, 6 samples were prepared and tested. Comparing the data attained from both monolithic and fiber embedded samples at varying UAM processing energies, a quantitative assessment of the effect of embedding both coated and uncoated fibers on the mechanical strength of these contact points can be achieved.

During the peel testing, the covering Al 3003 H18 foil layer was peeled from the start point of the consolidation at a loading rate of 50 mm/min until the load had fallen below 10% of the maximum. A schematic of the peel test apparatus is located in Fig. 4 and was installed onto an Instron 3366 tensile test machine fitted with a 1kN load cell. Performing the same process for the remaining samples allowed for an average maximum peel load to be calculated. Monolithic samples were prepared at both UAM parameter combinations and peeled in the same manner as the samples containing embedded fibers. This experimentation allows a value of the average peel resistance of the metal matrices to be calculated and used to calculate any potential change in mechanical strength as a result of the fiber embedding process.

2.5.2. Linear Weld Density (LWD) measurement

The influence of metallic fibers coatings and UAM processing energy on the mechanical strength of the metallic matrix was also investigated through an assessment of the Linear Weld Density (LWD). Linear Weld Density (LWD) can be defined as the length of a particular interface that appears properly bonded, divided by the total interface length inspected [20];

$$\text{LWD } (\%) = \frac{L_b}{L_i} \times 100$$

where L_b = bonded area length and L_i = bonded interface length respectively

The decision to calculate LWD is better understood when it is considered that UAM parts typically display unbonded regions or 'voids' along the interlaminate region. Determination of the LWD is often used to develop optimum process parameters for UAM builds [4,5,12,29]. Furthermore an understanding of LWD is important when considering the porosity of a UAM structure and its mechanical properties in the build direction [26]. It is generally considered that a higher LWD leads to improved bond quality in UAM structures. In most UAM builds, LWD density ranges from 40–95% [20].

For each of the fibers selected for this work, a total of 6 samples were prepared at each UAM energy combination. Furthermore, 6 monolithic samples were prepared at each UAM energy combination in order to act as a comparative reference. Both the fiber embedded and monolithic samples were cross-sectioned perpendicular to the fiber axial direction. Samples were taken from the beginning, middle and end sections across two identical substrates before being mounted in an epoxy resin (Fig. 5a). Following mounting, the samples were ground and polished to a 0.02-micron finish. A Nikon Optiphot optical microscope fitted with a GXCAM-5 ISH500 5.0 MP imaging system at 100× magnification was employed to image regions of the third and final Al 3003 H18-Al 3003 H18 weld interface (Fig. 5b). For each mounted sample, a total of ten images were taken from the same locations across the length of the welded Al 3003 H18 interface, either side of the central fiber. The overall LWD for each sample was then obtained by averaging the LWD values for each individually imaged section.

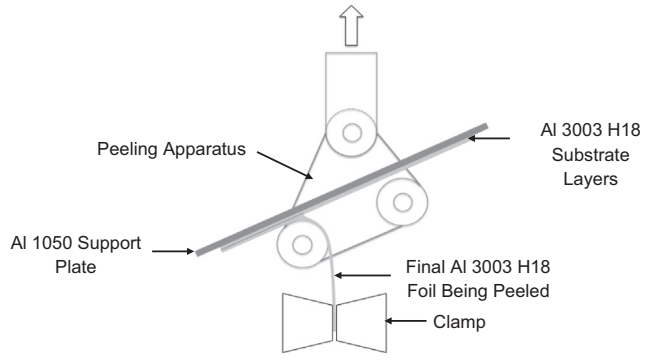

Fig. 4. Schematic diagram of peel apparatus with a UAM structure loaded.

2.5.3. Examination of the effect of UAM on the metallic fiber coating

In order to enhance the visualization of the metallic coating applied to the selected fibers, a Keller's (0.5% HF) etching solution was applied to the exposed polished surface of the previously prepared samples. Following standard procedures for etching, the samples were submerged in the Keller's etchant, with agitation, for 30 s per sample. Six samples were imaged for each fiber-UAM process energy combination. A Leica DM6000 M imaging system at 100× magnification was employed with both Bright Field and Dark Field illumination techniques as a means of highlighting the result of applying UAM to both Copper and Aluminum coated optical fibers of varying diameters.

To obtain greater levels of detail for the fiber/matrix interface Focused Ion Beam (FIB) milling for imaging was implemented in order to machine and then image a trench running parallel to the coating-matrix interface. This imaging was a means of determining if the coating was mechanically encapsulated or metallurgically bonded. Through the use of a Nova 600 Nanolab Dual Beam Focused Ion Beam Scanning Electron Microscope, a 10 μm wide, 15 μm long and 10 μm deep trench was milled parallel to the coating-matrix interface for each of the 6 coated fiber samples and imaged at up to 32,500×.

3. Results and discussion

3.1. Fiber light transmission testing

At both the HP and LP UAM processing parameters, the metal-coated optical fibers were capable of transmitting light with minimal power loss. In contrast, the uncoated fiber samples failed to transmit light at both the HP and LP UAM processing parameters due to fracturing of the silica core at the start and end points of embedment. The uncoated fibers were observed to either fracture during the welding process or soon as they were manipulated after embedding. This was not the case with the coated fibers, which remained intact and capable of transmitting light even when taken through a wide range of angles (Fig. 6). All of the coated fibers were shown to lose an average of ~2 dB of signal power after embedding, with no obvious differences between fibers coated with the Al or Cu. This degree of loss is minimal and similar to the expected attenuation losses from splicing/conectorising of fibers (ca. 0.5–1 dB loss). These losses are attributed to both bending losses as a result of fiber deviation within the UAM matrix, as well as scattering losses resulting in structural inhomogeneity's and defects in the core/cladding as a result of the action of the sonotrode on the fiber. There was no discernible difference in the transmission intensity varying between the LP and HP UAM processing parameters. This indicates that the quality of embedding at the matrix/-fiber interface is not necessarily an important factor in the fibers

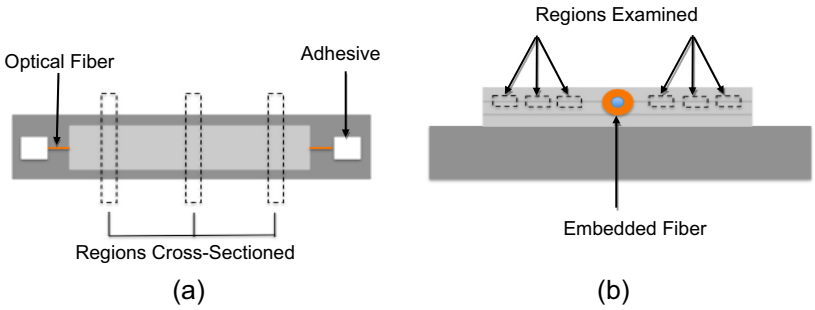

Fig. 5. (a) Selected regions cross-sectioned for microscopic imaging (b) example of a typical weld interface examination for the determination of LWD. (For interpretation of the references to color in this figure legend, the reader is referred to the web version of this article.)

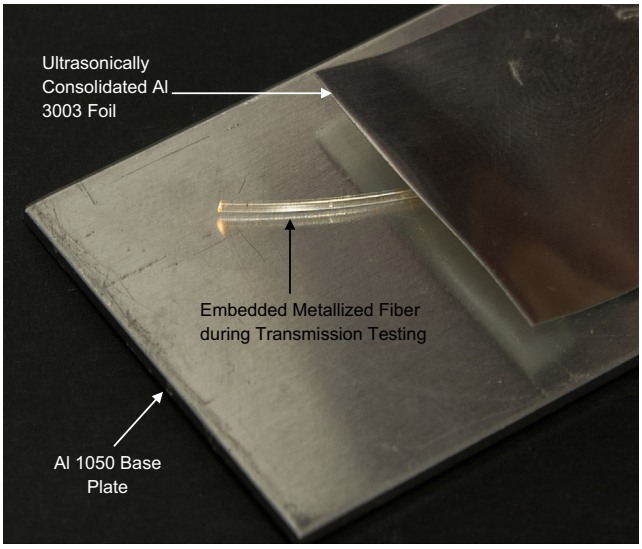

Fig. 6. Transmission testing of optical fiber post ultrasonic welding. (For interpretation of the references to color in this figure legend, the reader is referred to the web version of this article.)

ability to transmit light post encapsulation and the voids present at LP do not introduce additional losses.

The ability to maintain full fiber functionality whilst using high UAM processing energy is a significant step forward in the area of Smart MMCs. These new higher strength, fully functional UAM MMCs will enable a greater range of potential applications to be investigated such as; structural fatigue monitoring, harsh environment monitoring and advanced telecommunications integrated into high value Aluminum componentry.

3.2. Linear Weld Density analysis

The average Linear Weld Density (LWD) for each Fiber/UAM Energy combination was determined through microstructural analysis of mounted cross-sections. These average values are displayed in Fig. 7. A comparative reference using monolithic samples was included to highlight any potential change in bonding characteristics as a result of the inclusion of optical fibers within the UAM matrix. The general trend observed was that the HP UAM parameters resulted in a higher LWD (between 16% and 27%) for all fiber types. Despite both an increase in fiber size and the addition of metal surface coatings, the metal-coated fiber samples average LWD remains within 2% of the monolithic samples at the HP UAM parameters and 6% at lower UAM energies. It was also noted that in comparison to the LP parameters, the higher UAM energy parameters showed a more consistent level of consolidation quality as indicated by the lower standard error in the results. At both processing parameter combinations, the metal-coated optical fiber samples produced LWD's comparable to both uncoated and monolithic samples. The result of this is a UAM structure showing near full weld density, whilst still exhibiting full optical fiber functionality at processing parameters higher than previously thought possible.

Larger non-bonded sections or voids were prominent in those samples produced using lower contact pressures and oscillation amplitudes. Fig. 8 highlights a typical example of these non-bonded regions under a bright light-imaging field. The reduction in LWD displayed by all samples types at LP UAM parameters (ca. 20% average reduction across whole sample set) were anticipated based on prior literature [5,12,26]. Reductions in contact pressure and oscillation amplitude lead to accompanying reductions in interfacial stress between mating foils. This in turn reduces interfacial friction and the degree of plastic deformation observed in the foils, two key requirements in the formation of metallurgical bonds in UAM. The addition of fibers into the interlaminate regions leads to further reduction in LWD observed for the metal-coated fiber samples, although at LP UAM parameters this is more apparent. The additional size of the protective coating to the circumference of the metalized fiber samples (45–95 μm) further reduces the intimate contact between upper and lower foils that is required for bonding and as such, lower LWD are observed for metal-coated samples at LP UAM parameters than their uncoated counterparts. At HP UAM parameters, the increased contact pressures and oscillation amplitude are significant enough to overcome this effect and produce friction and plastic deformation of the foil great enough that LWD analogues to monolithic samples are observed.

The uncoated fibers superior performance at lower UAM energies relative to that of the metal-coated fibers (ca. 5% average reduction across whole sample set) is attributed to two key factors; reductions in the diameter of the uncoated fiber led to increased localized pressure in the areas local to the silica fiber. This increase in localized pressure led to high degrees of plastic deformation around the region local to the fiber, serving to increase the LWD by allowing more intimate contact between upper and lower foils. Secondly, due to the energy required to displace/deform the coating material being more significant at lower UAM energies, a larger proportion of the UAM energy delivered to the substrate is not utilized in bonding and is instead used in this coating removal process. At HP UAM parameters, the energy delivered to the substrate was not only great enough to displace the coating, but still provides the required energy for bonding (detailed in Section 3.5).

HP UAM parameters were previously shown to be too high to allow for the encapsulation of uncoated optical fibers within Aluminum matrices [14]. These increased parameters were shown to produce higher LWD across all samples when compared to the LP UAM parameters set (the threshold determined by Kong in

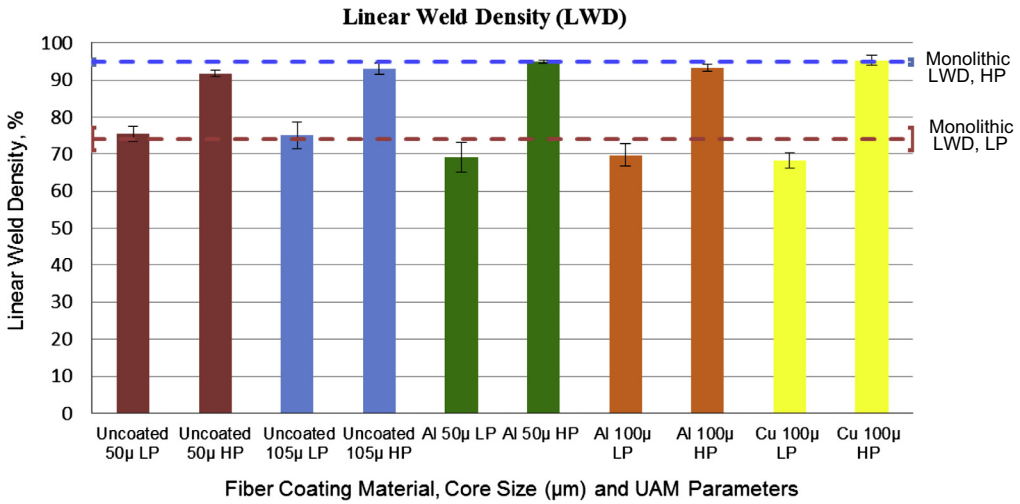

Fig. 7. Graphical representation of the Linear Weld Density (LWD) of both coated and uncoated fiber types at two UAM energy parameter combinations (HP and LP). Monolithic reference lines are included at both energy combinations. (For interpretation of the references to color in this figure legend, the reader is referred to the web version of this article.)

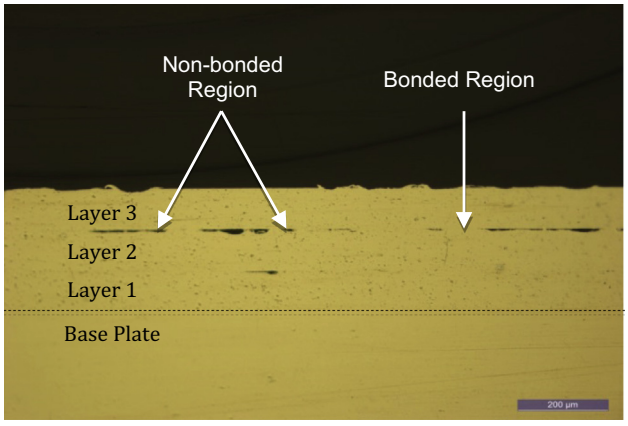

Fig. 8. Example cross-section analyzed for a determination of the Linear Weld Density (LWD) of a UAM sample highlighting the voids at the weld interface. (For interpretation of the references to color in this figure legend, the reader is referred to the web version of this article.)

the encapsulation of uncoated fibers). A higher LWD is generally thought to lead to a less porous UAM structure with improved bond qualities and mechanical strength [26]. At 95%, the level of LWD observed in the metal-coated samples prepared using higher UAM energies is at the upper echelons of what is considered to be a high level of bonding in UAM. Therefore through the metallization of the optical fiber, high degrees of LWD can be achieved comparable to that of monolithic samples whilst not compromising the functionality of these structures. This is a result not previously possible when dealing with standard uncoated optical fibers.

3.3. Mechanical peel testing

The determination of Linear Weld Density in itself does not provide a full assessment of the interlaminar bond quality in UAM. Direct imprint of the sonotrode topography onto the UAM substrate can lead to regions of intimate contact between upper and lower foils, which are indistinguishable from each other, but are not metallurgically bonded [28]. This can cause discrepancies in LWD analysis due to difficulties in differentiating these areas from genuinely bonded regions. As a result it is pertinent to further assess the bond quality achieved in the UAM structures through mechanical peel testing.

The third and final Al 3003 foil consolidated was peeled from the underlying substrate through mechanical peel testing. The average resistances to peeling are displayed in Fig. 9. In agreement with the average LWD's, higher UAM energy combinations were shown to produce an increase in the mechanical strength of the consolidated interface. The metal-coated fibers possessed bond strengths comparable to both monolithic samples (up to 6% reduction in peel resistance) and uncoated optical fiber samples (up to 10% reduction in peel resistance) at these higher UAM energies whilst at lower UAM energy parameters; the results are seen to substantially deviate from the peel resistances of monolithic samples. The metal-coated samples demonstrated reductions in mechanical strength of up to 29% at these lower settings. They did however remain on par with their uncoated counterparts at both parameter sets. The increase in weld force, amplitude and speed also brought with it a change in peeling profile from a brittle failure mode at higher UAM parameters, to a more ductile failure mode at lower UAM energy parameters.

In UAM substrates containing embedded fibers, several groups have noted work hardening of Aluminum matrices during consolidation [10,21]. Work hardening is a phenomenon that results in increases in strength of a material by increasing dislocation density. Through the action of plastic flow observed in UAM, dislocations display higher density with an accompanying reduction in mobility. As a result, increases in material strength and hardness are observed. At higher contact pressures and oscillation amplitudes this effect is amplified due to increasing degrees of plastic flow observed in the matrix material resulting in a harder, stronger material post-processing. When the covering Al 3003 foil is peeled from the underlying substrate in the high UAM energy substrates, the consolidated regions are now stronger than the surrounding local foil. When a bonded region is stronger than the local foil that region will fracture before being peeled. For this reason the substrates prepared at HP UAM parameters fracture at a similar force as work hardening results in a consolidated region stronger than the initial Aluminum material.

Lower UAM energies produce not only reduced degrees of plastic flow during UAM, but also lower Linear Weld Density's (LWD's) (Fig. 7). The result of which were both weaker bonding and fewer locations along the weld interface where new metallurgical bonds were formed (Fig. 10). Therefore substantially lower resistances to peeling (ca. 15%) are seen at these lower UAM energies than are seen at high UAM energy parameters. The deviation of the peel

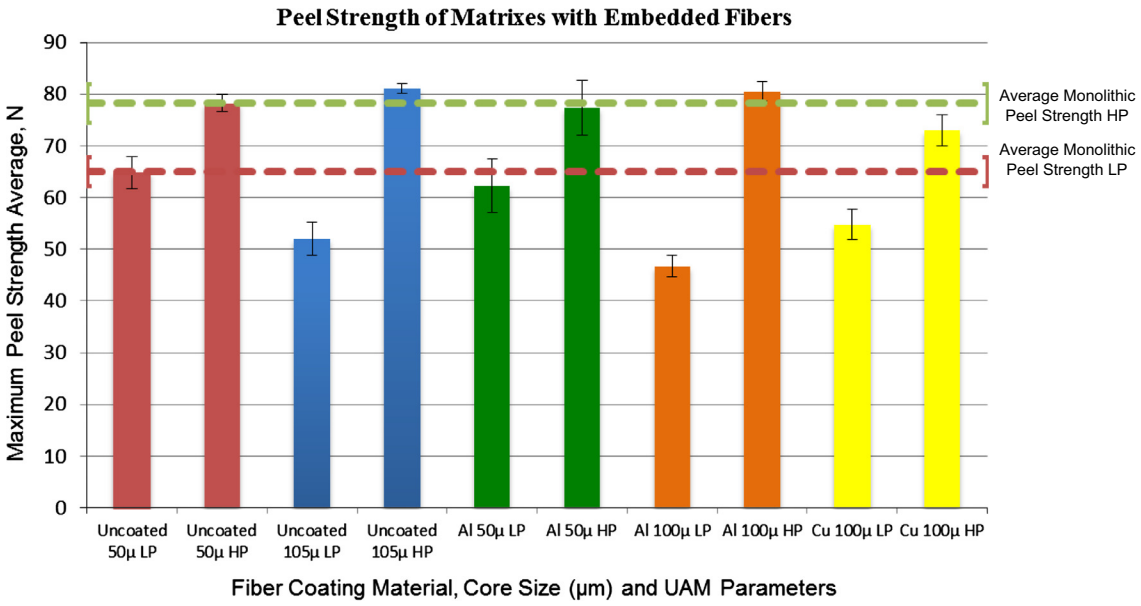

Fig. 9. The average resistance to peeling for both coated and uncoated optical fiber samples at both UAM energy processing parameters. Reference values and standard deviation of results are included for all sample types. (For interpretation of the references to color in this figure legend, the reader is referred to the web version of this article.)

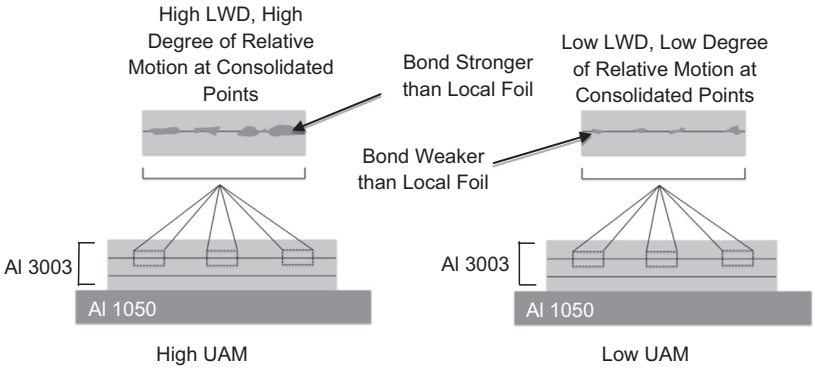

Fig. 10. Demonstrates the effect of varying degrees of UAM Energy on the bonding characteristics of Al 3003.

strength away from monolithic values in the case of samples prepared using LP UAM parameters contradicts those results obtained in the LWD analysis. If the linear weld density is within a few% of the monolithic sample as was shown, it would be expected that their peel strength would be similar. However large reductions were seen in peel strength that could be attributed to the transfer of sonotrode topology increasing the apparent LWD of the substrate whilst not increasing the degree of interlaminar bonding.

Prior to peeling, it was noted that in the case of the higher UAM energy parameters the foil strength was higher in the center of the substrate than at the edges. Often the foil laid directly over the embedded fiber remained attached to the foil directly beneath it, forming an enclosure around the fiber. The presence of the fiber in the central region of the substrate invokes and effect known as 'the edge effect' [10]. When fibers are placed directly underneath a covering foil, applied loads and oscillation energies are directed into smaller regions directly surrounding the fiber. The fibers narrow dimensions increase the pressure applied to the local area when compared to monolithic samples. As a consequence, the relative loads of oscillation energies around the fiber will increase relative to the load difference between the central region of the substrate and the edges. Therefore during peeling, the foil along the edges is prone to fracturing, leaving the fibers encapsulated and protected by the surrounding Aluminum matrix. This effect was amplified in the case of the metal coated fibers potentially due to bonding of the coating to the surrounding matrix further resisting the action of peeling (Section 3.4). This effect allowed for enhanced protection of the fiber even in the case of delamination.

Further analysis of the 'tear teeth' produced in peel testing of samples supports the finding that these higher UAM energy parameters result in stronger interlaminate bonding. Generally longer tear teeth indicate weaker bonding in UAM substrates. Fig. 11(a–d) shows several peel profiles generated by a selection of the prepared substrates. The strength increase at the center of these substrates appeared amplified in the case of uncoated optical fibers. The amplification of this effect is thought to be a result of a reduction in fiber size increasing the degree of localized pressure around the fiber leading to increased foil deformation and work hardening in the areas local to the fiber. This will have led to quicker fracture of the foil at higher UAM parameters.

The small degree of mechanical strength degradation observed in the metal-coated fiber embedded samples at high UAM energies indicated that not only are the weld density's comparable with monolithic samples, but so too is the mechanical strength. Both of these desirable factors come at no cost in regards to the structural integrity of the fiber and its ability to transmit light. Ultimately, the application of the protective metal coating allows

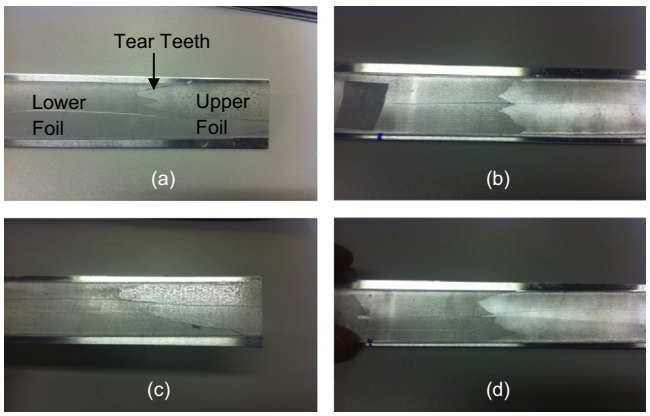

Fig. 11. Images highlighting the different peel teeth produced by different UAM energy parameters (a) 50 μm uncoated fiber low UAM energy (b) 50 μm uncoated fiber high UAM energy (c) 105 μm uncoated fiber low UAM energy (d) 105 μm uncoated fiber high UAM energy. (For interpretation of the references to color in this figure legend, the reader is referred to the web version of this article.)

for a UAM Metal Matrix Composite (MMC) to be formed that is not only mechanically strong as a result of higher processing parameters, but it is still capable of carrying out its required task, something that was previously not possible [14].

3.4. Topography of covering foil

As a result of surface roughness, when two foils come into contact, 100% intimate contact is not possible and there will inevitably be non-contact regions. Ram et al. reported that reductions in surface roughness can lead to the production of denser parts with fewer deformities/voids along the weld interface, thus increases in LWD and mechanical strength of laminate structures is observed [30].

Through a direct measure of the surface roughness exhibited by covering Al 3003 foil layers, differences in the encapsulation process between coated and uncoated optical fibers could be understood. The topography of the covering Al 3003 foil was successfully analyzed through the use of an Alicona InfiniteFocus IFMG4F surface profiling system and the acquired data studied through the use of Talymap Platinum 5.0 software. The average surface roughness, R_a, for each Fiber-UAM Energy combination was calculated and the results displayed in Fig. 12. The average roughness of monolithic samples is included to act as a reference for any topographical change as a result of the embedding process. Both Copper and Aluminum coated fibers were shown to have substantially lower R_a values in comparison to the monolithic samples (42% reduction in the case of both UAM energy parameters). Reductions in R_a were also observed when compared to the uncoated optical fiber samples (33% in the case of higher energy UAM and 32% in the case of low energy UAM parameters). Sample surface profiles obtains from both monolithic and fiber embedded samples are displayed in Fig. 13.

The observed reduction in surface roughness appeared to arise as a result of the application of a metal coating to the circumference of the fiber can be explained through two approaches; Firstly the lack of protective coating around the circumference of the fiber in the uncoated samples results in direct contact between upper foil and the silica core. It is conceivable that the greater the compressive strength difference between the foil and the secondary phase fiber, the higher the localized pressure around the fiber will be. As a result of these increased pressures, the region local to the fiber will exhibit a larger resultant force to the sonotrode and in turn aid the transfer of the sonotrode topology to the surface of the Aluminum. A second possibility for the reduction in surface roughness of metal coated samples compared to both monolithic and uncoated optical fiber samples is due to movement of the upper foil during consolidation. As the sonotrode passes directly over the covering foil, the UAM energy is transferred not only to the covering foil but also to the protective coating surrounding the fiber. As the coating is displaced, the circumference of the fiber is reduced by a distance equal to twice the thickness of the coating. This will result in a downward movement of the foil by a distance of potentially up to 230 μm.

Whilst on a single fiber scale this reduction in roughness is unlikely to have a substantial effect of the consolidation quality of future layers, it is conceivable that as the number of embedded fibers increases, so too will the disparity between uncoated and coated sample surface roughness. Large degrees of surfaces roughness are likely to lead to reductions in weld density and bond quality in these fiber dense UAM composite structures. The reduction in

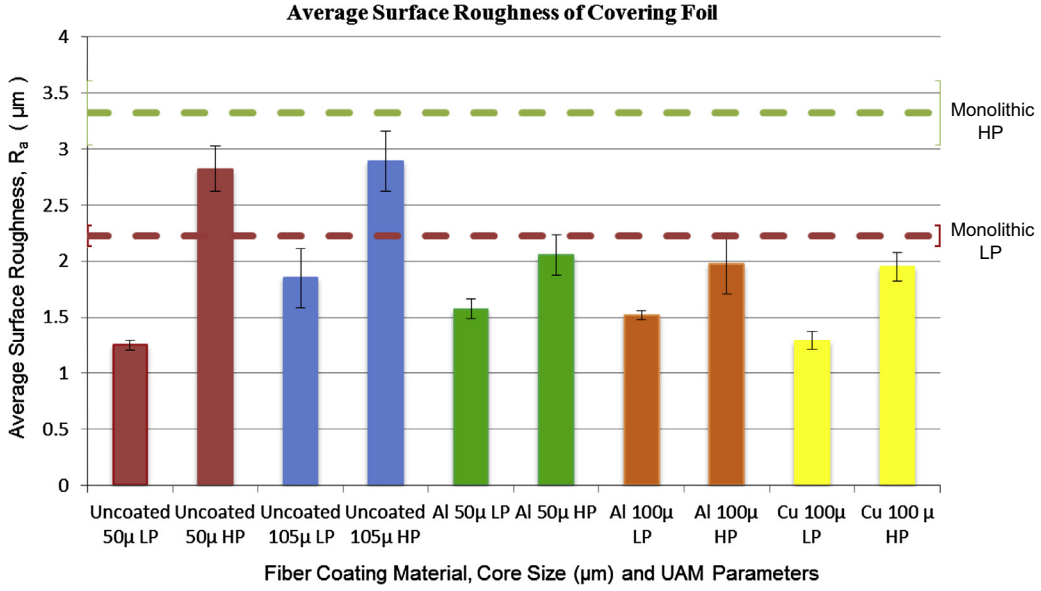

Fig. 12. Graphical representation of the average surface roughness of the covering Al 3003 foil layer. Monolithic reference lines are included at both energy combinations. (For interpretation of the references to color in this figure legend, the reader is referred to the web version of this article.)

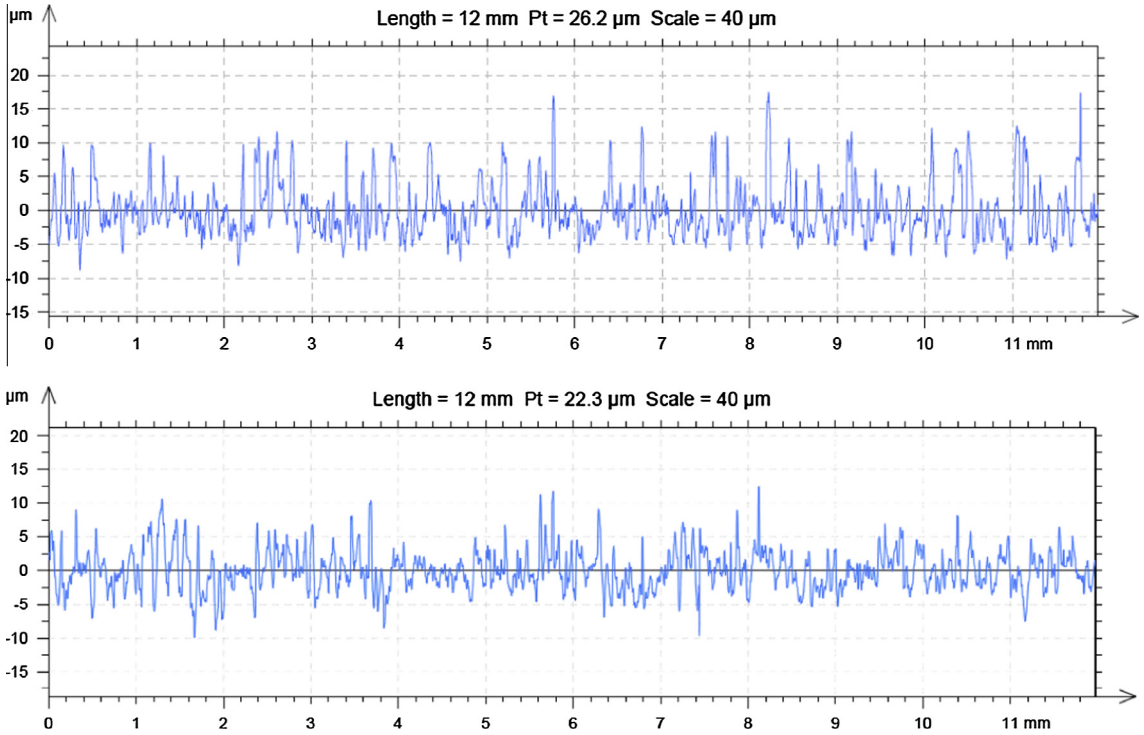

Fig. 13. Surface profiles of both monolithic and fiber embedded samples and high UAM processing parameters (HP). (For interpretation of the references to color in this figure legend, the reader is referred to the web version of this article.)

surface roughness exhibited by metal-coated optical fiber samples, whilst still maintain high degrees of welding density and mechanical strength, not only results in a high quality composite structure in the interlaminate region containing the fiber itself, but also allows for future layers to be deposited onto a more ideal surface for UAM.

3.5. Effect of UAM embedment on metal-coated optical fibers

The effects of applying varying degrees of UAM energy to optical fibers fitted with a protective metal coating was investigated through microstructural analysis of mounted cross-sections. Examination of the cross-sections showed that in the consolidation process, the metallic coating is displaced from the fibers circumference to a region a short distance away from the fiber and along the consolidation interface (the range varied from a few µm in the case of low UAM parameter combination to >150 µm in the case of the high UAM energy combination). Fig. 14 details examples of both Copper and Aluminum coated fiber samples embedded at both UAM energy parameters.

Utilization of higher energies resulting in displacement of the Aluminum coating between 150 and 200 µm from the

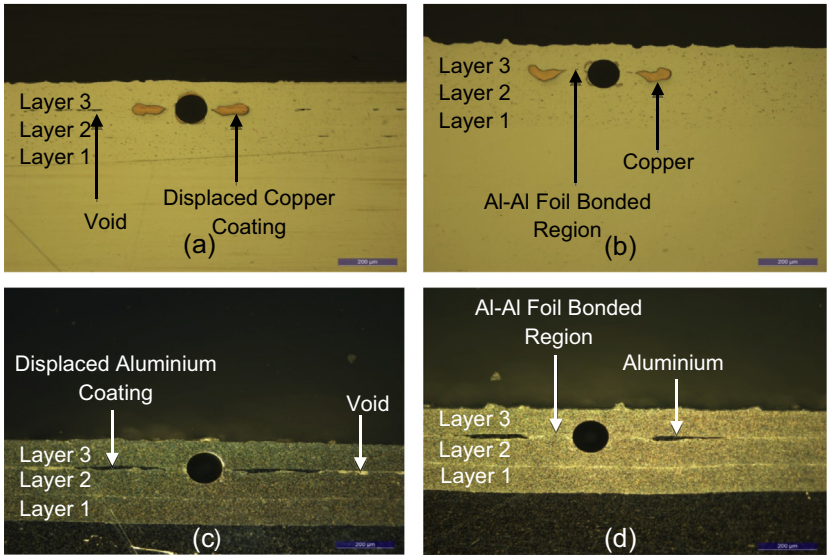

Fig. 14. Images of cross-section samples of different fiber coating material highlight the effects of both different material properties and processing parameters on the fiber embedding process. (a) Copper coating – Low UAM energy (b) Copper coating – High UAM energy (c) Aluminum coating – Low UAM energy (d) Aluminum coating – High UAM energy. (For interpretation of the references to color in this figure legend, the reader is referred to the web version of this article.)

circumferences of the fiber, whilst at lower processing energies displacements of 10–50 μm were visible. Similarly in the case of the copper coating, distances of 50–100 μm were shown for the higher contact pressures and oscillation amplitudes and 10–30 μm for the lower UAM energy parameters. Complete plastic flow was induced in the Aluminum matrix surrounding the core of the fibers as indicated by the regions of intimate contact between upper and lower foil directly around the silica core of the optical fiber. This allows for intimate contact of the light transmitting silica core with its surround metal matrix, forming a structurally sound metal matrix composite with low levels of porosity. Overall no earing of barrelling effects were observed at or around the fibers, although some voids were noted in the samples prepared at lower processing energies (Fig. 14a and c).

By altering the UAM processing energy, marked differences were observed in the interlaminate region for both coated fiber types. Similarly as large degrees of movement are noted in some regions of the Aluminum foils as a result of plastic flow, large degrees of movement are seen in the coating material. Increasing the total amount of UAM energy delivered to the substrate and the fiber resulted in an increased in the deformation and displacement distance of the protective metallic coating. By increasing the contact pressure and oscillation amplitude, the degree of movement of foils and interfacial stress in the interlaminate region is also increased. The effect of this increase is to place further stress directly onto the coating material, and as it is stripped from the central silica fiber, deposit it further from the circumference of the fastened silica core. These results differ substantially from results obtained by Li et al. in their work in the embedding of nickel coated optical fibers through ultrasonic spot welding [19]. Their work demonstrated that in the case of static spot welding, the nickel coating remained directly attached not only to the circumference of the fiber, but it also retained its original shape. This difference is attributed to the material properties of the protective metal coatings. In the ultrasonic welding of similar or dissimilar metal combinations, it is seen that the harder the material, the higher the degree of energy required to produce metallurgical bonds [31]. Therefore Nickel (Mohs hardness value of 4) is seen to deform to a lesser extent than both Copper (Mohs hardness value of 3) and Aluminum (Mohs hardness value of 2.5) in the process of ultrasonic welding. It could be that the action of using a rolling weld horn as opposed to a static probe to consolidate foils itself is the cause for the removal of the protective coating, and as a result this will be further investigate by utilizing UAM to embed Nickel coated optical fibers at a range of processing energies.

It is this difference in material properties of both Copper and Aluminum that further accounts for the difference in the interlaminar region of substrates fitted with different protective coatings. The increased hardness of copper relative to aluminum means that it is effect to a lesser to by UAM energy during consolidation. As a result, the copper coating is deposited both closer to the circumference of the silica core and is less deformed from its original geometry than those fibers fitted with Aluminum coatings (up to 100 μm difference at higher UAM energies and 20 μm at lower UAM energies).

Through the use of FIB and Scanning Electron Microscopy (SEM), highly magnified images at the coating-matrix interface revealed that the coating material is apparently bonded to the surrounding Al matrix (Fig. 15). The use of FIB–SEM as opposed to standard SEM affords the ability to visualize the 3-dimensional sections the coating-matrix interface and determine if consistent levels of bonding are exhibited throughout the composite structure. Merely visualizing the surface would not make this possible and it is also possible that the action of polishing/grinding the surface could lead to apparent intimate contact or cause micro fractures along the interface. The realization that the removed coating material is in fact bonded to the surrounding matrix was rationalized through the increased pressures brought about by action of the sonotrode directly to the circumference of the fiber

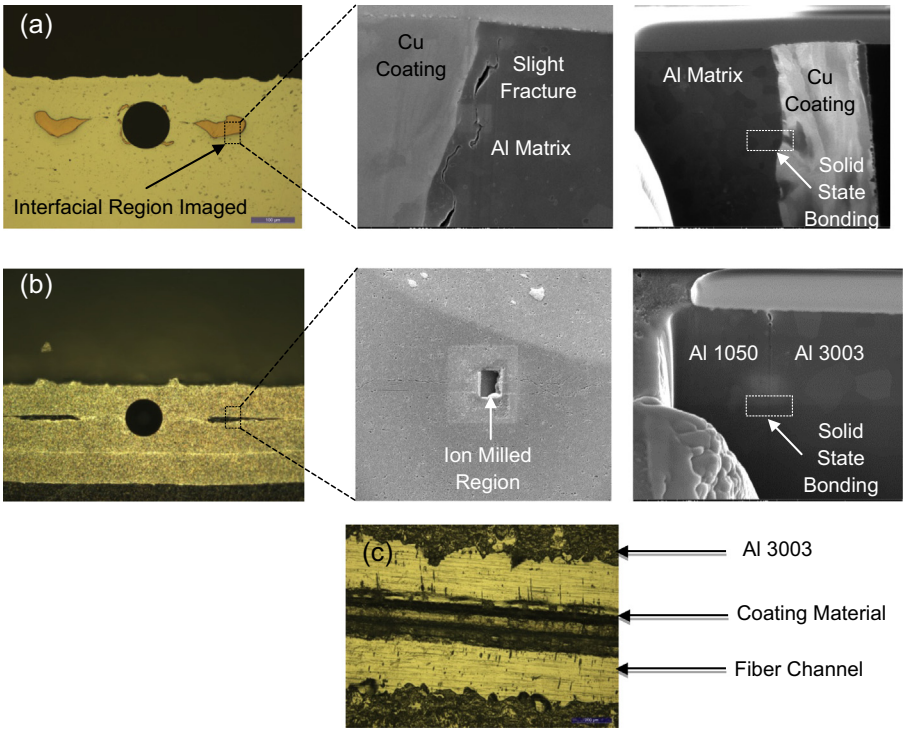

Fig. 15. (a) Focused Ion Beam (FIB) dual Scanning Electron Microscope (SEM) images of the Copper coating – Aluminum foil interface. (b) Images of the Al 3003 coating material – Al 1050 foil interface. (c) Image of dispersed coating visible on the surface of the substrate after mechanical peel testing. (For interpretation of the references to color in this figure legend, the reader is referred to the web version of this article.)

as opposed to the larger surface area of the substrate. These increased pressures result in higher UAM energies than those directly controlled by the operator and as a result, bonding combinations that are not usually possible at these UAM parameters can be realized. This was further evident in analysing the surface of the second Al 3003 foil deposited after peel testing. Areas of both copper and Aluminum were evident on the surface of the foil directly around the channel created by the fiber. Small signs of cracking were evident along the coating/matrix interface but were not noted around the fiber/matrix interface. This observation is significant in that if cracking at the fiber/matrix interface was observed, then increased fiber losses could arise due to waveguide scattering losses resulting from changes in the refractive index of the materials in direct contact with the fiber.

The effect of this apparent bonding is a reduction of the Width of Embedded Area (WEA) to that equivalent of uncoated optical fiber samples i.e. the WEA is now just the width of the silica fiber. Some fracturing along the coating-upper foil interface was noted in some samples. This is attributed to oscillation-induced movement of the upper foil during UAM causing small fractures in the Aluminum directly adjacent to the Copper–Aluminum bond. Further investigation into the effect of this bonding on the grain structure of both the surrounding matrix and the coating material itself are required to fully investigate the bonding mechanism demonstrated here. The ability to encapsulate these metal-coated fibers at process parameters higher than previously possible and without increasing the WEA, allows for a composite structure to be formed with a bonding area equal to that of unprotected fibers and possessing equivalent mechanical strength. The coating not only appears to provide protection to the fiber during consolidation, but its removal also beneficial in the encapsulation process. If the coating were to remain around the circumference of the fiber it is likely that cracking/fractures in the upper foil would be visible due to the fibers large diameter (165 μm) relative to the thickness of the foil covering foil (100 μm). Furthermore the removal of this coating in no way appears to affect the mechanical strength of the fiber at the weld interface, as is apparent by their ability to undergo a variety of manipulations after encapsulation.

In addition to the experimental methodology, it was noted that the metallized fibers were much more compliant to physical manipulation after they were embedded within the UAM structure. Additional testing had been planned to further characterize the strength of the fiber/matrix interfacial bond and the condition of the fiber post encapsulation. Currently it is not possible to determine the degree to which the silica core of the fiber is held in place via mechanical encapsulation through the determination of its interfacial sheer strength. Optical fibers are prone to fracture before it is removed from the bulk matrix, and as such, no pull out testing method currently suffices. This will therefore be subject to further investigation as a means of quantifying the force at which the fiber is held in place.

4. Conclusions

The ability to encapsulate uncoated optical fibers within UAM metal matrices has previously been demonstrated to be limited to relatively low UAM energy parameters. Further, the action of UAM on the coating materials, and their removal as a consequence of this, renders these fibers virtually useless after encapsulation. This work has uniquely demonstrated that through the application of a protective metal coating to the circumference of these fibers, optical fibers can be encapsulated within an Al 3003 H18 matrix in a continuous manner, at UAM processing energies higher than previously possible. Both Copper and Aluminum coated fibers were successfully embedded at these higher processing energies produced weld densities and resistances to peeling close to that of monolithic UAM Al 3003 H18 samples. Both the composition of the coating material and processing parameters were shown to result in different weld interfaces, but the processing parameters were shown to have a marked effect of the weld density and mechanical strength of the fabricated UAM samples. The encapsulation of these materials produced results markedly different from previous works regarding the encapsulation of nickel coated optical fibers; this work is the first to identify the metal coating stripped and redistribution of the fiber coating materials. This was attributed to different material properties of the coatings and potentially the action of using a rolling weld horn as opposed to static pressure.

Analysis of the removed coating indicated that it was not mechanically interlocked as previously shown in other works, but was in fact metallurgically bonded to the Al 3003 matrix material. As a result, there is no increase in the Width of Embedded Area (WEA) and the mechanical strength of the parts is not compromised. Topography of the substrates prepared using metal-coated fiber samples were shown to be considerably lower than both monolithic samples and uncoated optical fiber samples. This is attributed to both a reduction in localized pressures resulting from increased fiber sizes as well as movement in upper foils as a result of the dispersion of the metal coating.

This work has shown that through the application of metal coatings to the circumference of optical fibers, high strength; fully functioning, smart MMC structures are achievable through the use of UAM. Through this novel encapsulation process, the functionality and strength of the embedded fibers is retained and can now allow for a variety of applications to be tested where previously they were not possible. Additionally, the robust nature of this technique and the high processing parameters it affords mean that this work could be extended to a range of materials such as stainless steel and high strength aerospace Aluminum alloys; further increasing its applicability in the formation of a new area of additively manufactured composite structures. Through the findings of this research work and the new found ability to successfully incorporate continuous metal coated optical fibers within an Al 3003 metal matrix, forays into areas such as structural fatigue/damage monitoring as well as real-time temperature, pressure and strain monitoring, in otherwise inaccessible locations, can now be investigated.

Acknowledgements

This work was supported by the Engineering and Physical Science Research Council (EPSRC) via the Centre for Innovative Manufacturing in Additive Manufacturing. We would also like to thank AMS Technologies Ltd for their kind support during this work.

References

[1] Dehoff RR, Babu SS. Characterization of interfacial microstructures in 3003 aluminum alloy blocks fabricated by ultrasonic additive manufacturing. Acta Mater 2010;58(13):4305–15.
[2] White DR. Ultrasonic consolidation of aluminum tooling. Adv Mater Process 2003;161:64–5.
[3] Hopkins CD, Wolcott PJ, Dapino MJ, Truog AG, Babu SS, Fernandez SA. Optimizing ultrasonic additive manufactured Al 3003 properties with statistical modeling. J Eng Mater Technol 2012;134(1):011004.
[4] Kong CY, Soar RC, Dickens PM. A model for weld strength in ultrasonically consolidated components. Proc Inst Mech Eng Part C J Mech Eng Sci 2005;219:83–91.
[5] Kong CY, Soar RC, Dickens PM. Optimum process parameters for ultrasonic consolidation of 3003 aluminium. J Mater Process Technol 2004;146:181–7.
[6] Edmonds HC, Harris RA. The effect of electro-discharge machined sonotrode topology on interlaminar bonding in ultrasonic consolidation. In: SPIE smart structures and materials + nondestructive evaluation and health monitoring; 2011. p. 797814–797814-13.

[7] Obielodan JO, Ceylan A, Murr LE, Stucker BE. Multi-material bonding in ultrasonic consolidation. Rapid Prototyping J 2010;16(3):180–8.
[8] Ram GDJ, Robinson C, Yang Y, Stucker BE. Use of ultrasonic consolidation for fabrication of multi-material structures. Rapid Prototyping J 2007;13(4):226–35.
[9] Koellhoffer S, Gillespie JW, Advani SG, Bogetti TA. Role of friction on the thermal development in ultrasonically consolidated aluminum foils and composites. J Mater Process Technol 2011;211(11):1864–77.
[10] Li D, Soar RC. Characterization of process for embedding SiC fibers in Al 6061 O matrix through ultrasonic consolidation. J Eng Mater Technol 2009;131(2):021016.
[11] Friel RJ, Harris RA. A nanometre-scale fibre-to-matrix interface characterization of an ultrasonically consolidated metal matrix composite. Proc Inst Mech Eng Part L J Mater Des Appl 2010;224(1):31–40.
[12] Yang Y, Janaki Ram GD, Stucker BE. An experimental determination of optimum processing parameters for Al/SiC metal matrix composites made using ultrasonic consolidation. J Eng Mater Technol 2007;129(4):538.
[13] Kong CY, Soar RC, Dickens PM. Ultrasonic consolidation for embedding SMA fibres within aluminium matrices. Compos Struct 2004;66(1–4):421–7.
[14] Kong CY, Soar R. Method for embedding optical fibers in an aluminum matrix by ultrasonic consolidation. Appl Opt 2005;44(30):6325.
[15] Siggard EJ. Investigative research into the structural embedding of electrical and mechanical systems using ultrasonic consolidation (UC); 2007.
[16] Christopher J. Robinson, B.E. Stucker, A.J. Lopes, R. Wicker. Integration of direct-write (DW) and ultrasonic consolidation (UC) technologies to create advanced structures with embedded electrical circuitry; 2006. p. 60–9.
[17] Majumder M, Gangopadhyay TK, Chakraborty AK, Dasgupta K, Bhattacharya DK. Fibre bragg gratings in structural health monitoring—present status and applications. Sensors Actuators A Phys 2008;147(1):150–64.
[18] Mou C, Saffari P, Li D, Zhou K, Zhang L, Soar R, et al. Smart structure sensors based on embedded fibre bragg grating arrays in aluminium alloy matrix by ultrasonic consolidation. Meas Sci Technol 2009;20(3):034013.
[19] Li Y, Liu W, Feng Y, Zhang H. Ultrasonic embedding of nickel-coated fiber bragg grating in aluminum and associated sensing characteristics. Opt Fiber Technol 2012;18(1):7–13.
[20] Schick AJCLDE, Hahnlen RM, Dehoff R, Collins P, Babu SS, Dapino MJ. Microstructural characterization of bonding interfaces in Aluminum 3003 blocks fabricated by ultrasonic additive manufacturing. Weld J 2010;89:105–15.
[21] Li D, Soar RC. Plastic flow and work hardening of Al alloy matrices during ultrasonic consolidation fibre embedding process. Mater Sci Eng, A 2008;498(1–2):421–9.
[22] Kumar S. Development of functionally graded materials by ultrasonic consolidation. CIRP J Manuf Sci Technol 2010;3(1):85–7.
[23] Davis JR, editor. Metals Handbook. Properties and Selection: Nonferrous Alloys and Special-Purpose Materials, Vol. 2. ASM International; 1990.
[24] Huang Y, Liang X, Azarmi F. Innovative Fiber optic sensors for pipeline corrosion monitoring. In: Pipelines 2014; 2014, p. 1502–11.
[25] Butov OV, Chamorovskii YK, Golant KM, Shevtsov IA, Fedorov AN. Fibers and sensors for monitoring nuclear power plants operation. In: Proceedings of SPIE – the international society for optical engineering; 2014, vol. 9157, p. 91570X.
[26] Janaki Ram GD, Yang Y, Stucker BE. Effect of process parameters on bond formation during ultrasonic consolidation of aluminum alloy 3003. J Manuf Syst 2006;25(3):221–38.
[27] Gonzalez R, Stucker B. Experimental determination of optimum parameters for stainless steel 316L annealed ultrasonic consolidation. Rapid Prototyping J 2012;18(2):172–83.
[28] Friel RJ, Johnson KE, Dickens PM, Harris RA. The effect of interface topography for ultrasonic consolidation of aluminium. Mater Sci Eng, A 2010;527(16–17):4474–83.
[29] Kong CY, Soar RC, Dickens PM. Characterisation of aluminium alloy 6061 for the ultrasonic consolidation process. Mater Sci Eng, A 2003;363(1–2):99–106.
[30] J. Ram, Y. Yang, J. George, C. Robinson, B.E Stucker . Improving linear weld density in ultrasonically consolidated parts. In: Proceedings of the 17th solid freeform fabrication symposium; 2006.
[31] Daniels HPC. Ultrasonic welding. Ultrasonics 1965;3(4):190–6.